ESA CONTRACT REPORT

Contract Report to the European Space Agency

Support-to-Science-Element (STSE) Study
EarthCARE Assimilation

WP-2200 report: Monitoring of lidar data

February 2013, updated February 2014

Authors: *S. Di Michele, E. Martins, M. Janisková*

ESA ESTEC contract 4000102816/11/NL/CT

European Centre for Medium-Range Weather Forecasts
Europäisches Zentrum für mittelfristige Wettervorhersage
Centre européen pour les prévisions météorologiques à moyen terme

ECMWF

Series: ECMWF ESA Project Report Series

A full list of ECMWF Publications can be found on our web site under:
http://www.ecmwf.int/publications/

Contact: library@ecmwf.int

European Centre for Medium Range Weather Forecasts
Shinfield Park, Reading, RG2 9AX, England

Contract Report to the European Space Agency

Support-to-Science-Element (STSE) Study EarthCARE Assimilation

WP-2200 report: Monitoring of lidar data

Authors: S. Di Michele, E. Martins, M. Janisková

ESA ESTEC contract 4000102816/11/NL/CT

February 2013, updated February 2014

ABSTRACT

A basic monitoring system for lidar observations has been put in place. Time series of cloud observations from the CALIPSO lidar and corresponding first-guess departures simulated from the ECMWF model have been generated. Their comparison has shown that using the model, quantities with smaller ranges of oscillation are monitored. The study has also demonstrated that cloud-top height derived from backscatter can be used as a monitoring variable. Results indicate that, by monitoring the time series of first guess departures, instrument/model anomalies can be identified when they exceed some typical range of variation. Thus, a set of threshold values are defined, on which a warning system could be based.

Contents

1 Introduction

The monitoring of observational data is a fundamental element for all operational data assimilation systems used by Numerical Weather Prediction (NWP) centres. Before the active assimilation of new data can take place, a necessary step is the check of the model-vs-observation statistics. At the European Centre for Medium Range Weather Forecasts (ECMWF), every new observation that is brought into the operational analysis system is first monitored for a period of time. This process also provides a unique tool to routinely check for instrument deficiencies using the model as a reference point. In fact, Hollingsworth et al. (1986) already provided a good evidence that short-term forecast errors (first-guess errors) are quite low, thus making possible to evaluate the data quality by comparison with the corresponding model first-guess. Noteworthy, not only operational satellites, but also the research ones can benefit from a monitoring activity: for instance Muñoz Sabater et al. (2012) recently used the ECMWF NWP model to assess the performance of the observations from the European Space Agency (ESA) mission Soil Moisture and Ocean Salinity (SMOS).

ESA is currently preparing the Earth, Clouds, Aerosols and Radiation Explorer (EarthCARE) research satellite, planned for launch in 2016. Among other instruments, it will carry a lidar (ATLID) and a cloud radar (CPR), thus providing observations of the vertical structure and the horizontal distribution of cloud and aerosol over all climate zones. Space-borne lidar and radar observations are currently from the CloudSat (Stephens et al., 2002) and CALIPSO (Winker et al., 2009) missions, launched in 2006 as part of the A-Train constellation. A number of studies, including the ESA-funded project Quantitative Assessment of the Operational Value of Space-Borne Radar and Lidar Measurements of Cloud and Aerosol Profiles (QuARL, Janisková et al., 2010), have shown that such observations have the potential to be assimilated into Numerical Weather Prediction (NWP) models and thus could contribute to improvement of the initial atmospheric state of Global Circulation Models (GCM). The current ESA-funded STSE study on EarthCARE has as main objective the development of an off-line tool to monitor/assimilate Level-1 cloud data from radar and lidar in the ECMWF system. This report summarizes the results of the work done in the context of WP-2200 of this project, that is the monitoring of lidar observations in clouds based on data from the CALIOP (Cloud-Aerosol Lidar with Orthogonal Polarization) lidar on board CALIPSO.

The monitoring studies have been performed considering the time evolution of CALIOP observations over a period of 30 days (January 2007) using selected statistics, namely mean, standard deviation and number of samples. These quantities have been evaluated gathering data over time windows of four different sizes: a single granule (i.e. half orbit), 12 hours (corresponding to the ECMWF 4D-Var assimilation window), 24 hours and a running average over a week (with a one-day stepping). The monitoring of the temporal evolution of a quantity was usually performed separating the observations over independent geographical regions. Doing so, possible different ranges of variation for observations, consequence of the different meteorological regimes, could be taken into account. As in the previous study for the radar observations, the separation has been done done distinguishing between tropical (from 30°S to 30°N) and mid-latitude observations, for the latter focusing on cases in the Southern hemisphere (from 60°S to 30°S). The reason for such selection was the aim to concentrate on observations over ocean in order to avoid issues with orography, and obviously more such cases are available in the Southern hemisphere than in the mid-latitudes of the Northern hemisphere.

The temporal evolution of CALIOP observations, considering both stand-alone cloud backscatter and first-guess (FG) departures (differences between observations and model equivalents) is described in Section 2. In Section 3, the feasibility of monitoring cloud-top height derived from backscatter measurements is then investigated. Conclusions are provided in Section 4.

2 Monitoring of lidar backscatter

In order to understand if there is any potential in routinely monitoring CALIOP observations against the corresponding quantities derived from the forecast model, statistics from CALIOP cloud backscatter and from the corresponding FG departures are investigated by comparing the range of variation of their temporal evolution.

2.1 Time series of CALIOP backscatter

The monitoring of lidar observations makes use of CALIOP observations (at 532 *nm*) in cloudy conditions. The selection of the range gates containing clouds is based on the information contained in the CALIPSO level-2 product called Vertical Feature Mask (Liu et al., 2009). The retained values of cloud backscatter are averaged onto the closest model grid point to match the horizontal resolution (25 km in our case) of simulated observations. In addition, range bins below 8.3 km are averaged in couples to get a uniform 60-meter resolution (from the original 30-m) along the vertical. A similar vertical sampling is obtained for simulations through regridding of the model atmospheric variables.

Figure 2.1 shows the temporal evolution of the number $n_{\beta_{CA}}$ of averaged cloudy CALIOP observations for six reference altitude levels at Southern mid-latitudes. The most evident feature is the sharp decrease of occurrences at days 12 and 13. This drop is due to the unavailability of CALIOP data because of a spacecraft manoeuvring and because of a Universal Space Network (USN) ground station anomaly occurred at those dates. An USN ground station problem is also the reason for the (less dramatic) decrease in data volume at day 28. Outside these periods affected by the mentioned technical issues, we note that the largest amount of data is between 10 km and 6 km, and decreases below. When considering the tropics, shown in Fig. 2.2, the largest portion of observations are above 8 km and (in much smaller amount) below 2 km. In both regions, we note that the number of cases entering the 12-hour slots presents significant oscillations (with variations of up to one thousand samples).

The temporal evolution of CALIOP mean cloud backscatter $\overline{\beta}_{CA}$ is displayed in Fig. 2.3 for the same six reference altitude levels as in Fig. 2.1, considering observations at Southern mid-latitudes. Plots contain means over the four chosen averaging time-windows, each indicated by a different line colour or dot. The comparison across levels highlights a clear distinction between the values of mean backscatter below and above 4 km. Above 4 km, the mean backscatter is usually below $10^{-2} km^{-1} sr^{-1}$, while below it can reach values up to five times higher. This increase can be attributed both to the larger amount of water content and to the presence of cloud in liquid phase, which corresponds to a signal return that is much stronger than the one of ice. A similar feature can be noted when considering CALIOP observations in the tropics, as displayed in Fig. 2.4. In this case, a rapid increase in mean backscatter occurs around an altitude height of 6 km. This can be explained by the higher vertical extent of clouds in this region. Table 2.1 gives, for each of the six reference levels under consideration, the difference $\Delta\overline{\beta}_{CA}$ between the maximum value and the minimum value of $\overline{\beta}_{CA}$ in the month. This quantity expresses the oscillation range of the mean backscatter and it was evaluated taking out the days (12, 13, 28) with reduced number of data, where statistics would be unreliable. As expected, Table 2.1 shows that the oscillation range of the mean backscatter always decreases as the averaging time windows increases and that there are large differences in range of variation between the two geographical regions.

The temporal evolution of the backscatter standard deviation $\sigma_{\beta_{CA}}$ is shown in Fig. 2.5 and Fig. 2.6 for mid-latitudes and tropics, respectively. We note that already the 12-hour averaging results in ranges of standard deviation quite stable in time and that there are large differences across altitude levels due to the different magnitude of the backscatter.

As done for the mean, we can define the oscillation range of the standard deviation $\Delta\sigma_{\beta_{CA}}$ as the difference between the maximum and the minimum values of $\sigma_{\beta_{CA}}$ in the month. The values, given in Table 2.2, show

again that also the fluctuations in backscatter standard deviation are reduced increasing the time window and that they are usually larger in the Tropics.

CALIOP	**Mid-Latitudes South**			**Tropics**		
$\Delta\overline{\beta}[km^{-1}sr^{-1}]$	*Granule*	*12 hours*	*Day*	*Granule*	*12 hours*	*Day*
h=12 km	0.0217	0.0070	0.0048	0.0250	0.0029	0.0022
h=10 km	0.0285	0.0044	0.0023	0.0311	0.0080	0.0051
h=8 km	0.0761	0.0104	0.0046	0.1218	0.0180	0.0128
h=6 km	0.1738	0.0282	0.0124	0.2567	0.2567	0.0715
h=4 km	0.3526	0.0552	0.0235	0.1984	0.0433	0.0308
h=2 km	0.3987	0.0905	0.0383	0.4622	0.0574	0.0463

Table 2.1: Oscillation range of CALIOP backscatter mean value at different time windows.

CALIOP	**Mid-Latitudes South**			**Tropics**		
$\Delta\sigma_\beta[km^{-1}sr^{-1}]$	*Granule*	*12 hours*	*Day*	*Granule*	*12 hours*	*Day*
h=12 km	0.0136	0.0089	0.0045	0.0158	0.0038	0.0026
h=10 km	0.0152	0.0044	0.0039	0.0251	0.0096	0.0046
h=8 km	0.0512	0.0151	0.0102	0.1161	0.0333	0.0204
h=6 km	0.1563	0.0408	0.0289	0.0875	0.0824	0.0622
h=4 km	0.2502	0.0604	0.0266	0.0948	0.0469	0.0313
h=2 km	0.2083	0.0792	0.0387	0.1530	0.0456	0.0340

Table 2.2: Oscillation range of CALIOP backscatter standard deviation evaluated at different time windows.

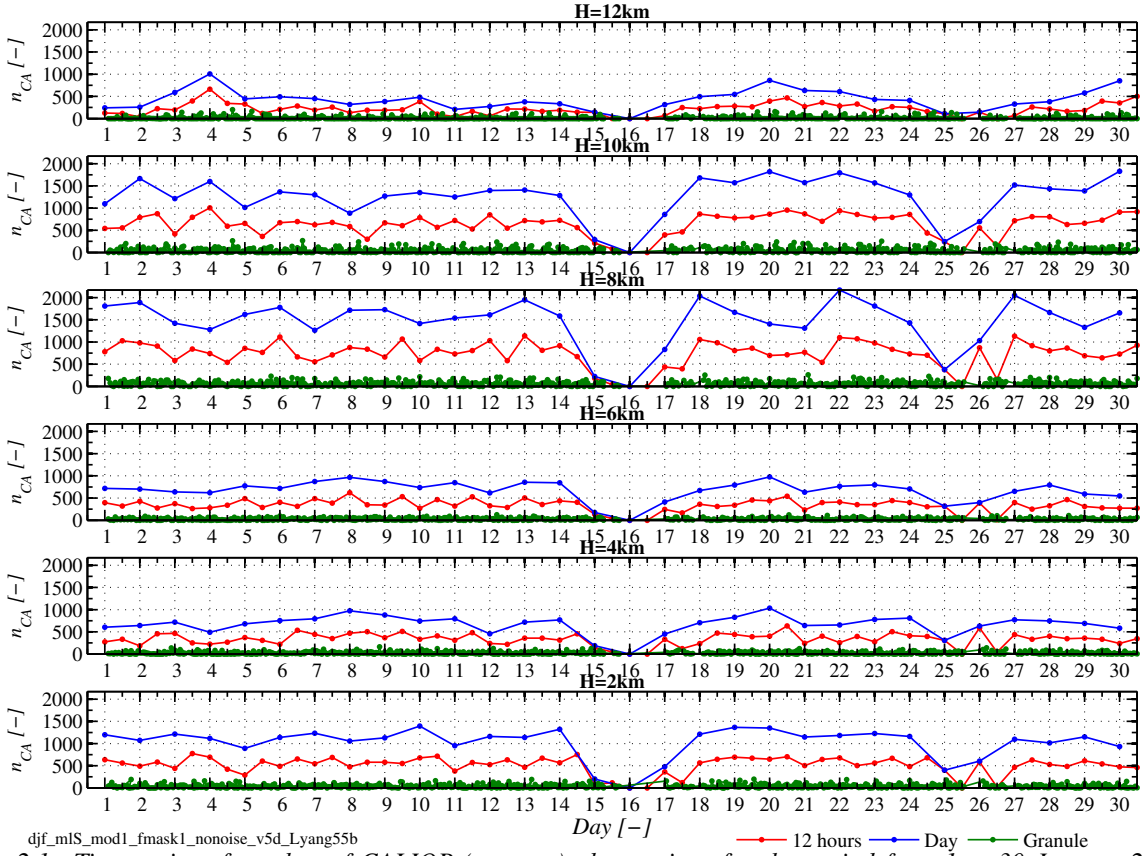

Figure 2.1: Time series of number of CALIOP (average) observations for the period from 1 to 30 January 2007, at mid-latitudes South (30°S-60°S). Each line refers to the time window stepping indicated in the legend. Different panels contains data at the altitude level (H) shown in the title.

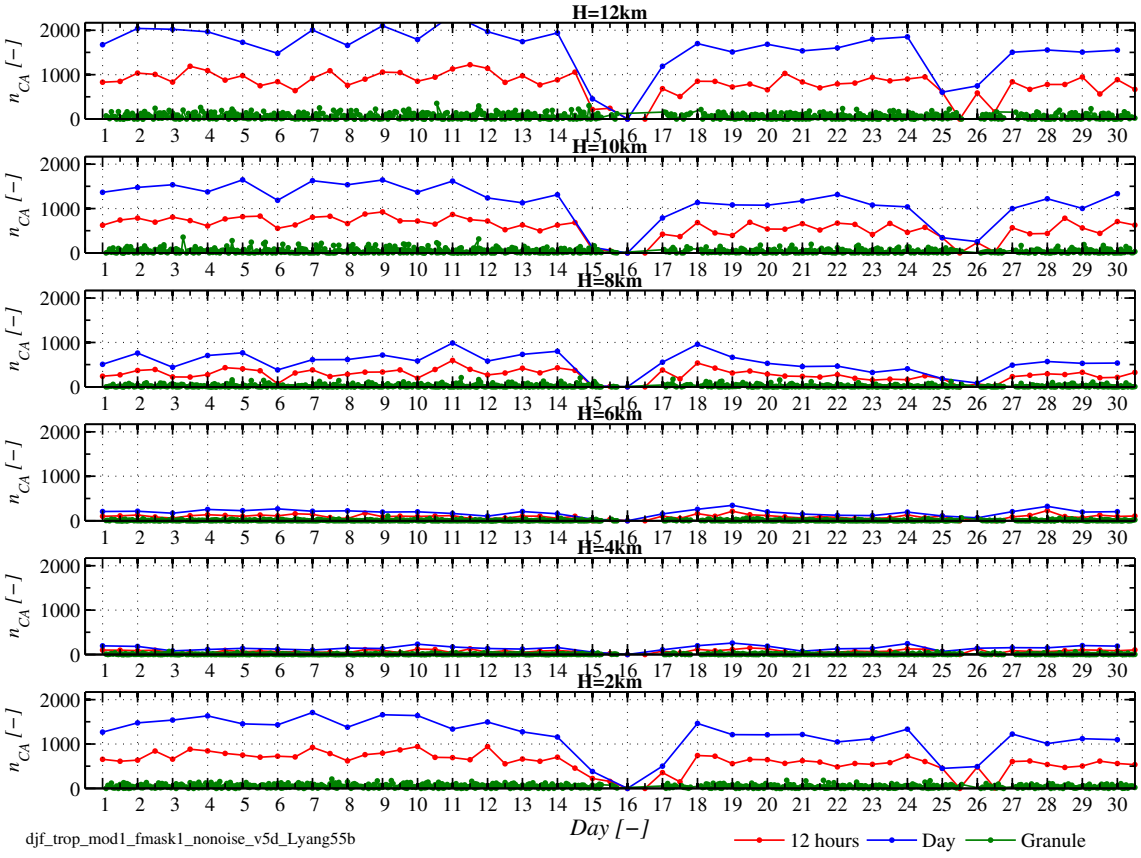

Figure 2.2: Same as Fig. 2.1, but considering observations in the tropics (30°S-30°N).

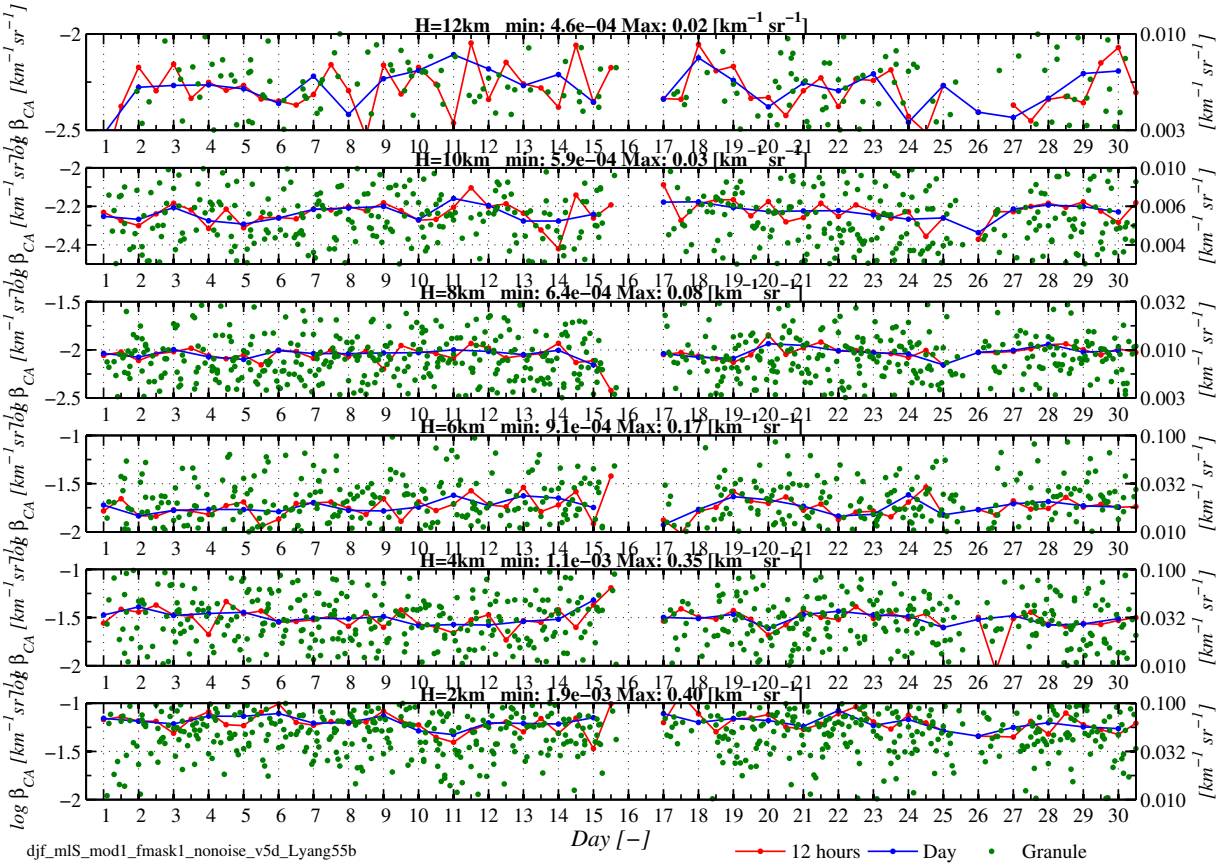

Figure 2.3: Same as Fig. 2.1, but for time series of mean CALIOP backscatter considering observations at mid-latitudes South (30°S-60°S).

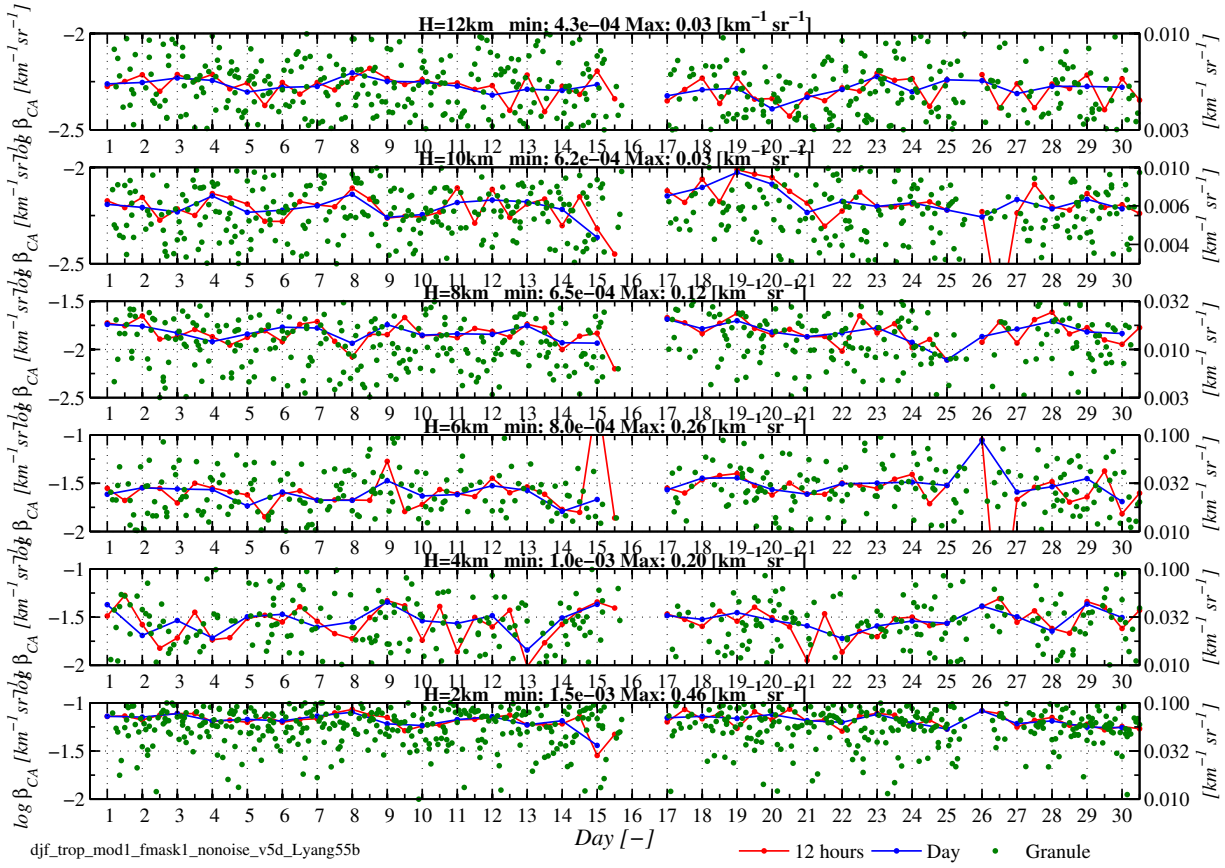

Figure 2.4: Same as Fig. 2.3, but considering observations in the tropics (30°S-30°N).

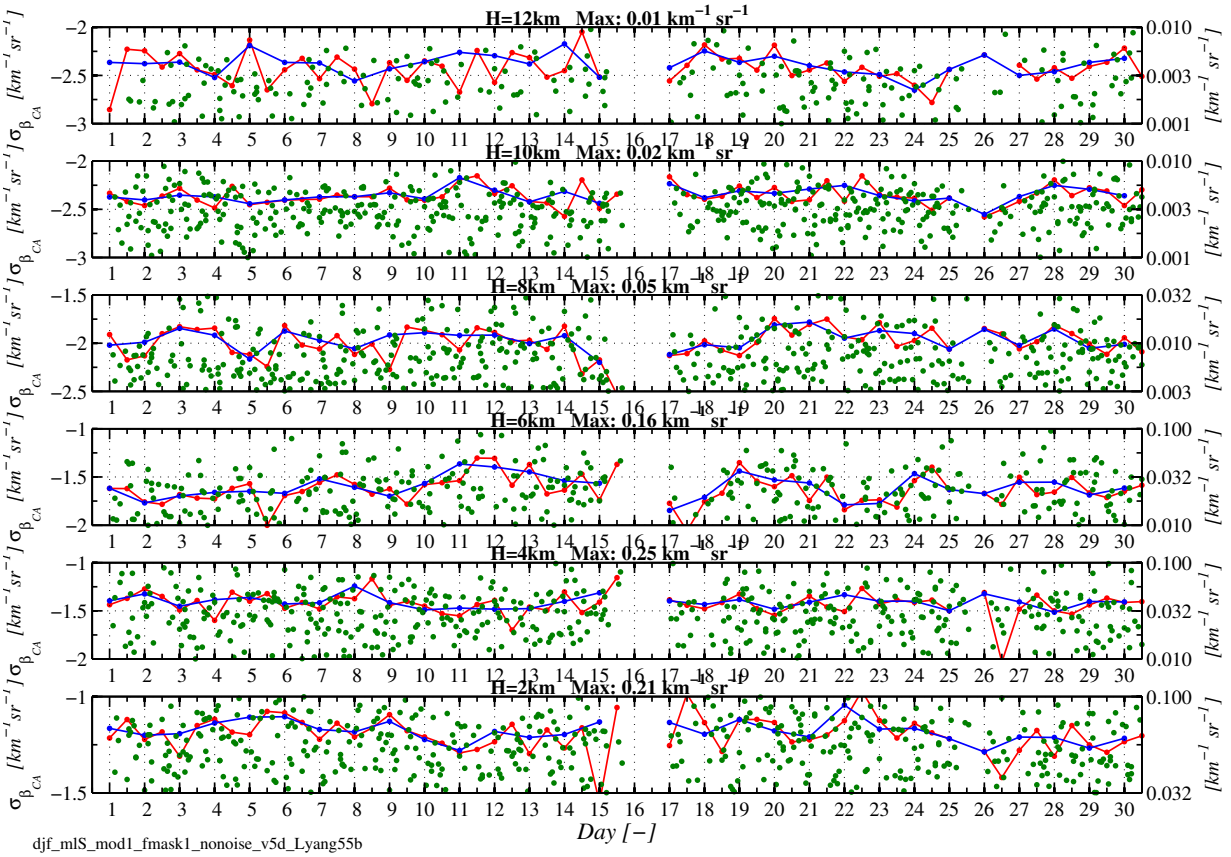

Figure 2.5: Same as Fig. 2.1, but for time series of CALIOP backscatter standard deviation considering observations at mid-latitudes South (30°S-60°S).

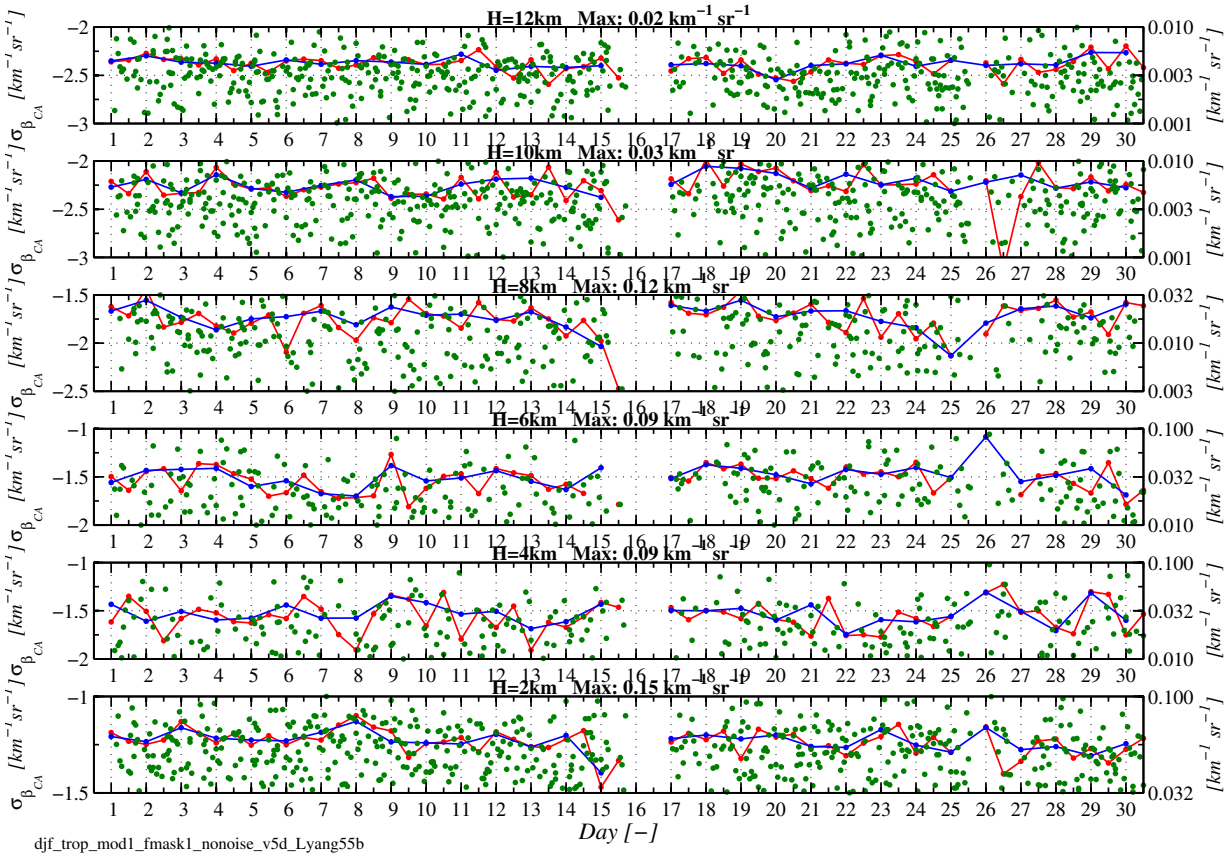

Figure 2.6: Same as Fig. 2.5, but considering observations in the tropics (30°S-30°N).

2.2 Time series of CALIOP backscatter FG departures

As done for CloudSat observations, an strategy for monitoring cloud backscatter in the context of an assimilation system has been investigated. In principle, if observations are accurately simulated by the NWP forecast model, a continuous monitoring of their differences would provide a better identification of problems in the data than it would be using only observations.

Figure 2.7 shows a qualitative comparison between CALIOP cloud backscatter observations (at 532*nm*) and their equivalent ZmVar simulations (Di Michele et al., 2014b) from the IFS short-term forecasts. Cloudy-only CALIOP observations (top panel) are obtained using the Vertical Feature Mask product (Liu et al., 2009; Vaughan et al., 2009) to remove range bins containing only molecular backscatter or affected by aerosols. The resulting data are then re-gridded and averaged to model resolution. The matched ZmVar simulations (bottom panel) show that the forecast model is able to realistically reproduce the main cloud structures. However, there are some evident differences in the backscatter intensity. In particular, the model, because of its much coarser horizontal resolution, is often unable to represent the most intense and finest structures.

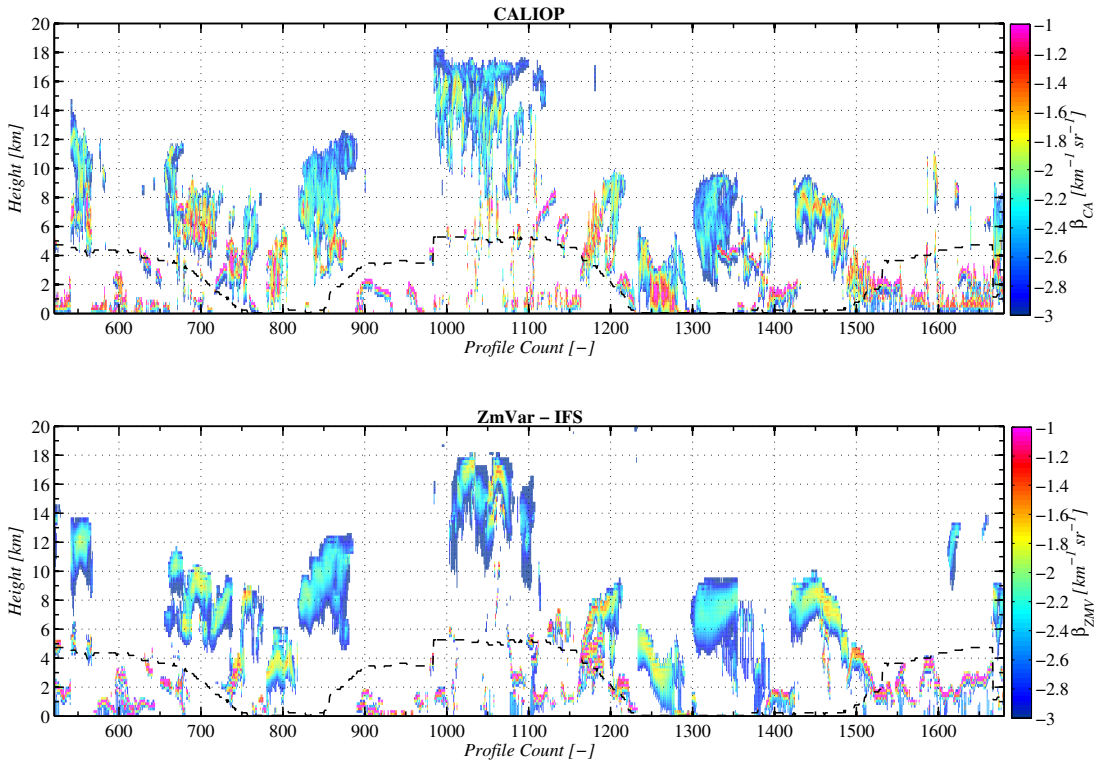

Figure 2.7: Top panel: Cloud backscatter (averaged to model resolution) observed by CALIOP on 1st January 2007. Bottom panel: corresponding values simulated by ZmVar using the ECMWF model short-term forecasts.

In order to properly evaluate if monitoring FG departures has some advantages over using observations alone, a screening procedure must be devised able to select the best observations to be used, removing the ones with a too large disagreement. These cases would otherwise have a negative impact on the monitoring statistics of FG departures.

For this study, a simple screening has been set up to retain only the cases with a sufficient good agreement. Based on the analysis above, we have decided to monitor only cases where both modelled and observed backscatter are larger than $2 \cdot 10^{-3} km^{-1} sr^{-1}$ if above 8 km and larger than $3 \cdot 10^{-3} km^{-1} sr^{-1}$ below 8 km. Also, given the poor agreement below 4 km, the monitoring will only consider observations at levels above this altitude.

The number of samples of FG departures $n_{\delta\beta}$ passed through quality control are shown in Fig. 2.8 for the Southern mid-latitudes. Comparing with Fig. 2.1, we note a percentage reduction of data of about 50% across all levels.

In Fig. 2.9 similar plots are given for observations at tropical latitudes over the same period. In this case, the majority of cases above 10 km are retained. Below, there is a screening of 50 % of data up to 4 km, while at 2 km the majority of observations of clouds are rejected. The heavy screening is a consequence of the disagreement between simulated and observed cloud backscatter, which tends to increase at levels below the cloud top. In fact, especially in the tropics, the lidar signal in clouds is considerably affected by attenuation, therefore errors in the attenuation at levels above the range-bin of interest (due to inaccuracies in the modelled cloud profile) give rise to large differences in the measured (attenuated) backscatter.

The time series of mean FG departures $\overline{\delta\beta}$ relative to observations at mid-latitudes South and tropics, are given in Fig. 2.10 and Fig. 2.11. The plots clearly show a smaller range of variation associated to the monitoring of FG departures. As done for $\overline{\beta}_{CA}$, we can consider the difference between the maximum and minimum values of the mean FG departures within the monitoring period, $\Delta\overline{\delta\beta}$. Based on Fig. 2.10 and Fig. 2.11, Table 2.3 contains the ratio (in percent) between the oscillation range of the mean FG departures $\Delta\overline{\delta\beta}$ and the one of the mean CALIOP observations $\Delta\overline{\beta}_{CA}$. We note that the range of variation of FG departures is always lower (e.g. below 100) than the one of the observations. The largest decrease (few percent) occur at lower altitudes, since the oscillation of observations alone are there one order of magnitude larger than at levels above, while (after screening) FG departures are limited to much lower oscillations.

The time series of the standard deviation $\sigma_{\delta\beta}$ of FG departures are shown in Fig. 2.12 and Fig. 2.13, respectively for Southern mid-latitudes and tropics. An oscillation range $\Delta\sigma_{\delta\beta}$ can be also defined for standard deviation departures, as the maximum of $\sigma_{\delta\beta}$ along the monitoring period. Table 2.4 gives the values of $\Delta\sigma_{\delta\beta}$ divided by $\Delta\sigma_{\beta_{CA}}$. Also for standard deviations, monitoring FG departures is preferable to observations alone since it gives a reduction in the oscillation range, allowing the detection of smaller anomalies. This conclusion is similar to the one obtained in Di Michele et al. (2014a) for the CloudSat and reaffirms the utility of having a model as a reference during monitoring of lidar/radar observations in clouds.

The analysis of time evolution of mean/standard deviation of temporally-averaged CALIOP observations or FG departures is very irregular when considering a single granule. This is a consequence of the very high horizontal resolution, but lack of a proper swath of the lidar: two successive granules usually contain observations of very different cloud structures or different portions of the same structure. As done for the CloudSat, it is worth investigating the correlation between the temporal evolutions of the granule-mean cloud backscatter observed by CALIOP and the one simulated by ZmVar to understand if this correlation is high enough to be used as monitoring quantity. Figures 2.14 and 2.15 show the temporal evolution of the correlations $c^{\beta}_{\pm 7}$, $c^{\beta}_{\pm 11}$ and $c^{\beta}_{\pm 15}$, evaluated over lengths of 7, 11 and 15 granules, respectively. One can notice that the variation of the temporal evolution is quite changeable even for the granule mean. Overall underestimation of the simulated backscatter compared to the observed values was presented in Di Michele et al. (2014b) (Section 4 of that report). This underestimation becomes more prominent going from higher to lower altitudes and it leads to correlations which rearly exceeds 0.6. Therefore for the lidar observations, an exploitation of the correlation in the context of monitoring is not recommended option.

CALIOP - IFS	Mid-Latitudes South			Tropics		
$\Delta\overline{\delta\beta}[km^{-1}sr^{-1}]$	*Granule*	*12 hours*	*Day*	*Granule*	*12 hours*	*Day*
h=12 km	0.0135	0.0078	0.0037	0.0125	0.0032	0.0019
h=10 km	0.0149	0.0029	0.0024	0.0227	0.0028	0.0019
h=8 km	0.0228	0.0039	0.0026	0.0257	0.0054	0.0039
h=6 km	0.0205	0.0043	0.0018	0.0355	0.0044	0.0033
h=4 km	0.0262	0.0050	0.0019	0.0277	0.0078	0.0050

Table 2.3: Oscillation range of the mean FG departures of CALIOP mean backscatter, given at different time windows.

CALIOP - IFS	Mid-Latitudes South			Tropics		
$\sigma_{\delta\beta}/[km^{-1}sr^{-1}]$	*Granule*	*12 hours*	*Day*	*Granule*	*12 hours*	*Day*
h=12 km	0.0102	0.0058	0.0052	0.0090	0.0050	0.0046
h=10 km	0.0092	0.0060	0.0050	0.0097	0.0053	0.0051
h=8 km	0.0115	0.0058	0.0056	0.0148	0.0063	0.0056
h=6 km	0.0141	0.0064	0.0059	0.0364	0.0081	0.0074
h=4 km	0.0309	0.0097	0.0089	0.0412	0.0100	0.0091

Table 2.4: Maximum standard deviation of FG departures of CALIOP backscatter standard deviation, given at different time windows.

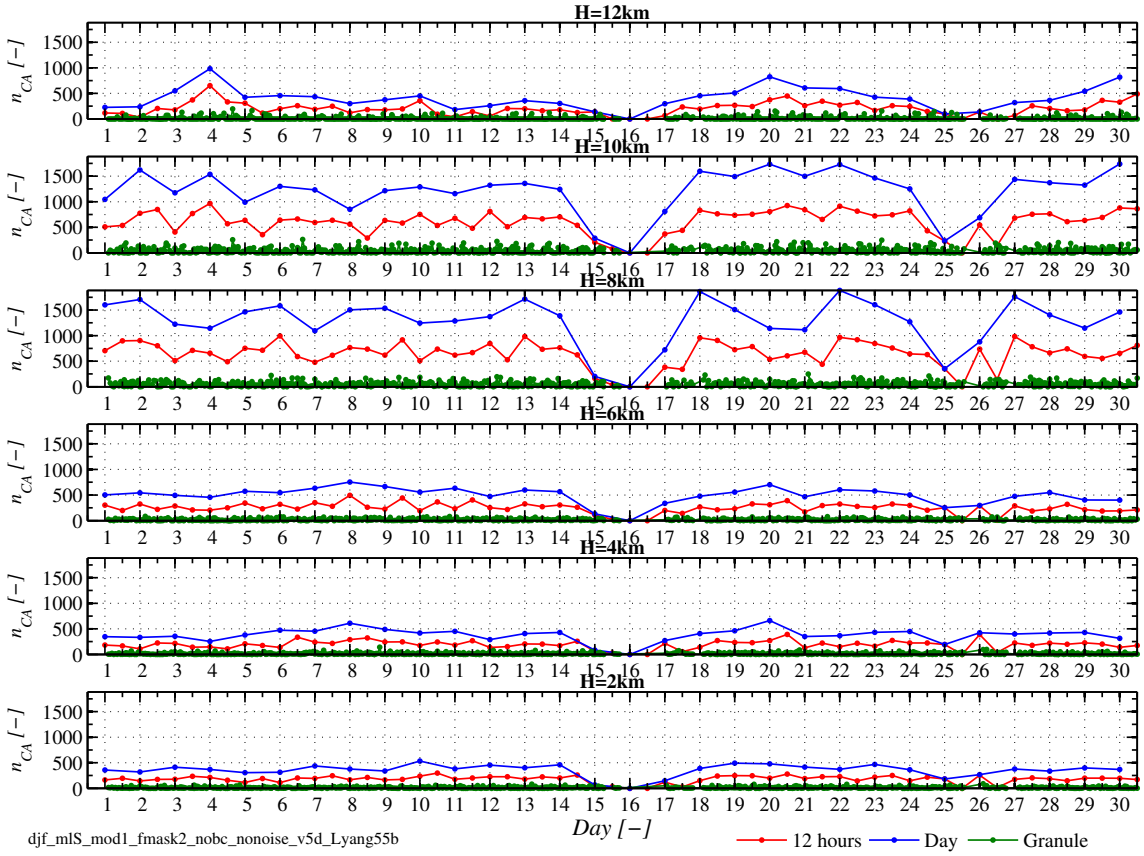

Figure 2.8: Same as Fig. 2.1, but after quality control.

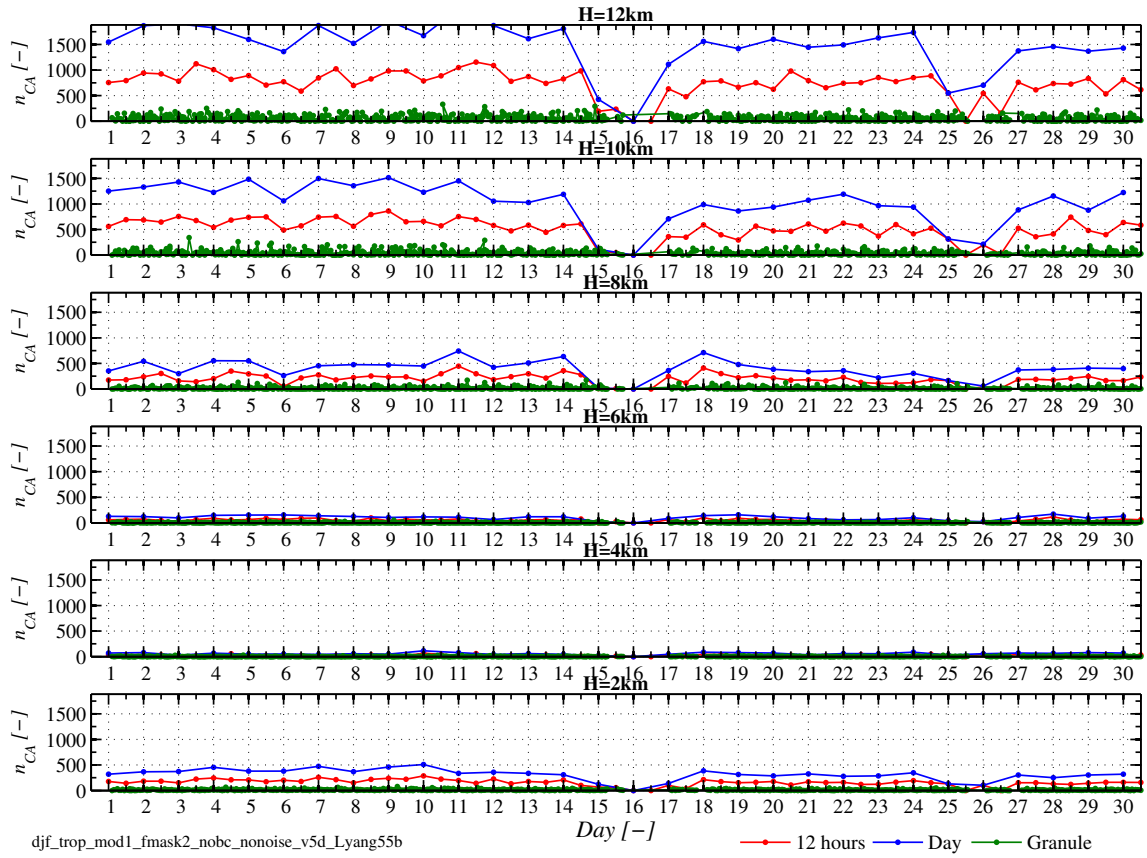

Figure 2.9: Same as Fig. 2.8, but considering observations in the tropics (30°S-30°N).

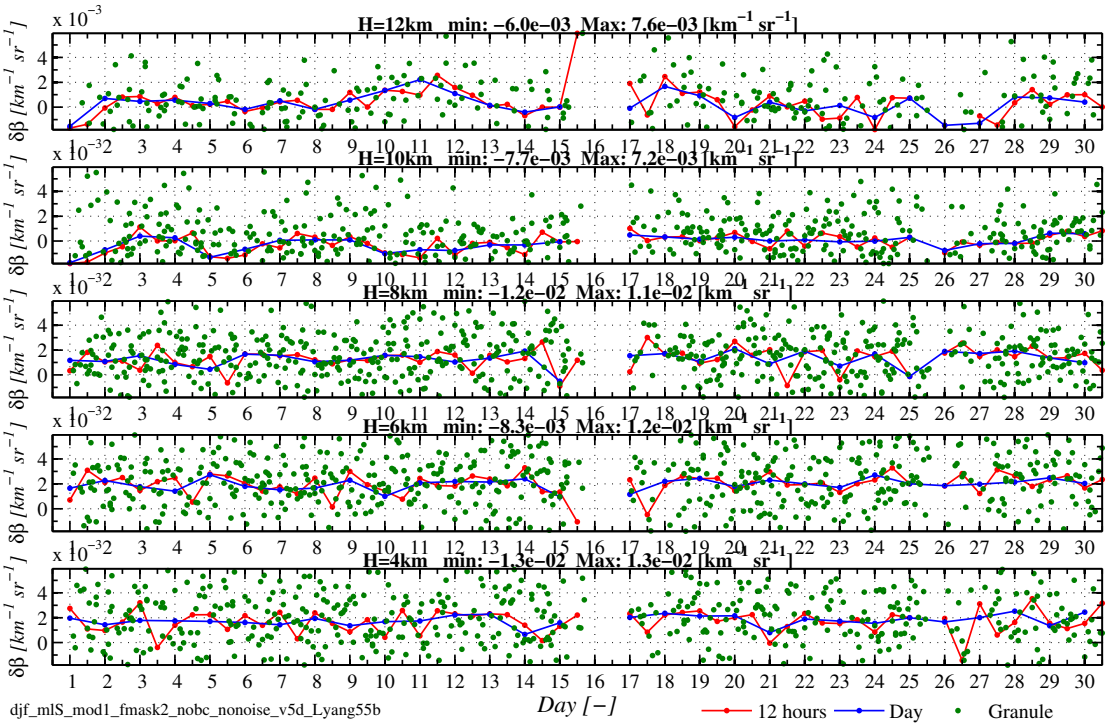

Figure 2.10: Same as Fig. 2.8, but for time series of mean CALIOP backscatter first-guess departures considering observations at mid-latitudes South (30°S-60°S).

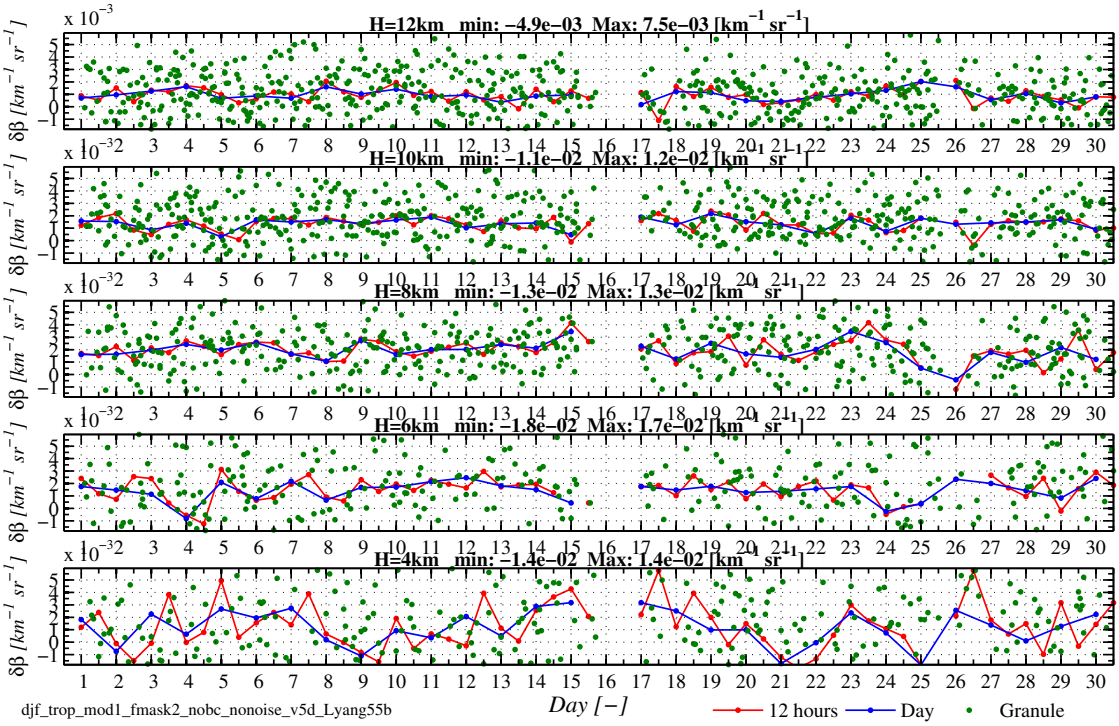

Figure 2.11: Same as Fig. 2.10, but considering observations in the tropics (30°S-30°N).

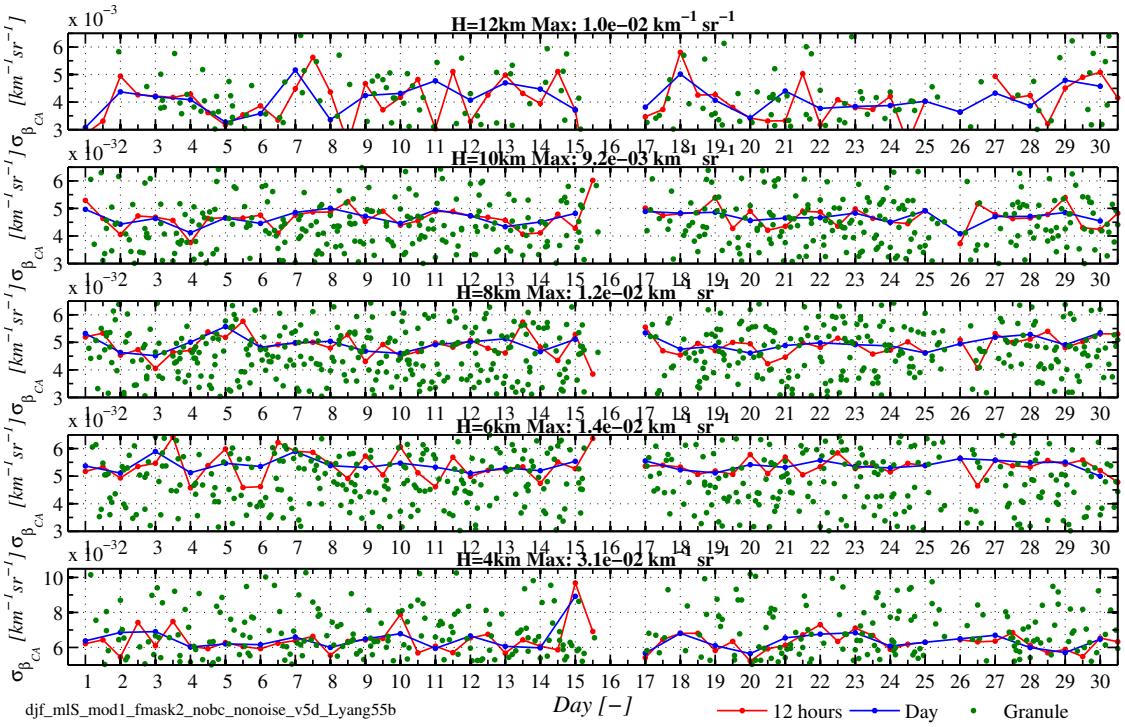

Figure 2.12: Same as Fig. 2.8, but for time series of CALIOP backscatter first-guess departure standard deviation, considering observations at mid-latitudes South (30°S-60°S).

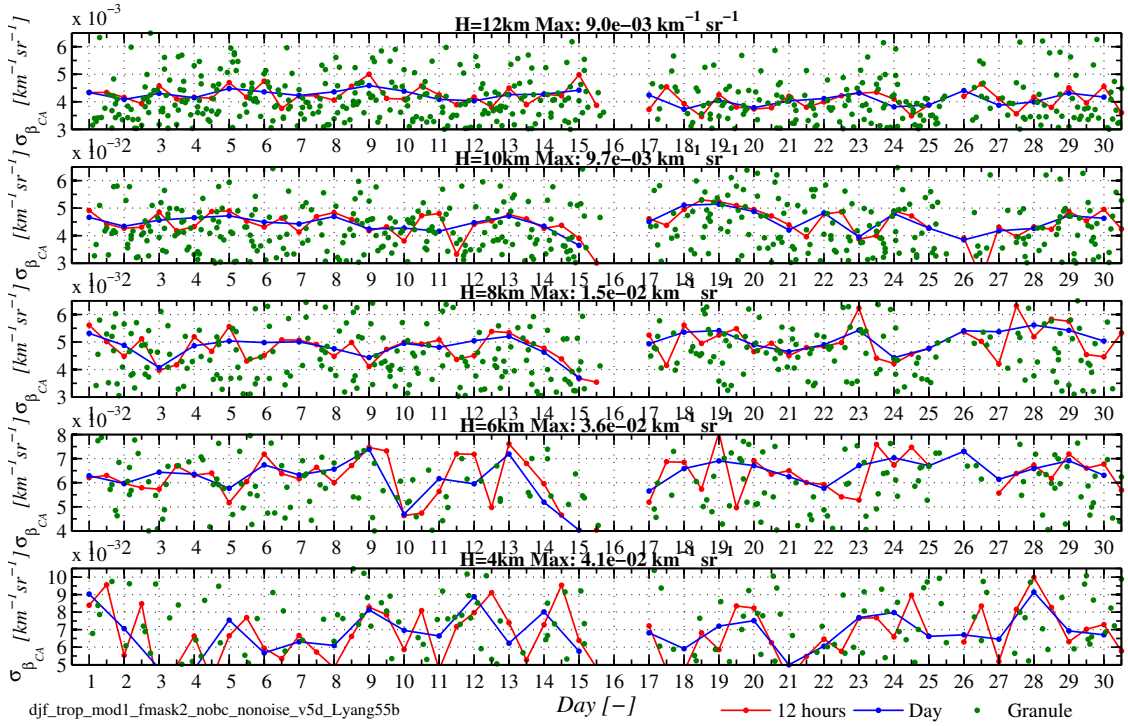

Figure 2.13: Same as Fig. 2.12, but considering observations in the tropics (30°S-30°N).

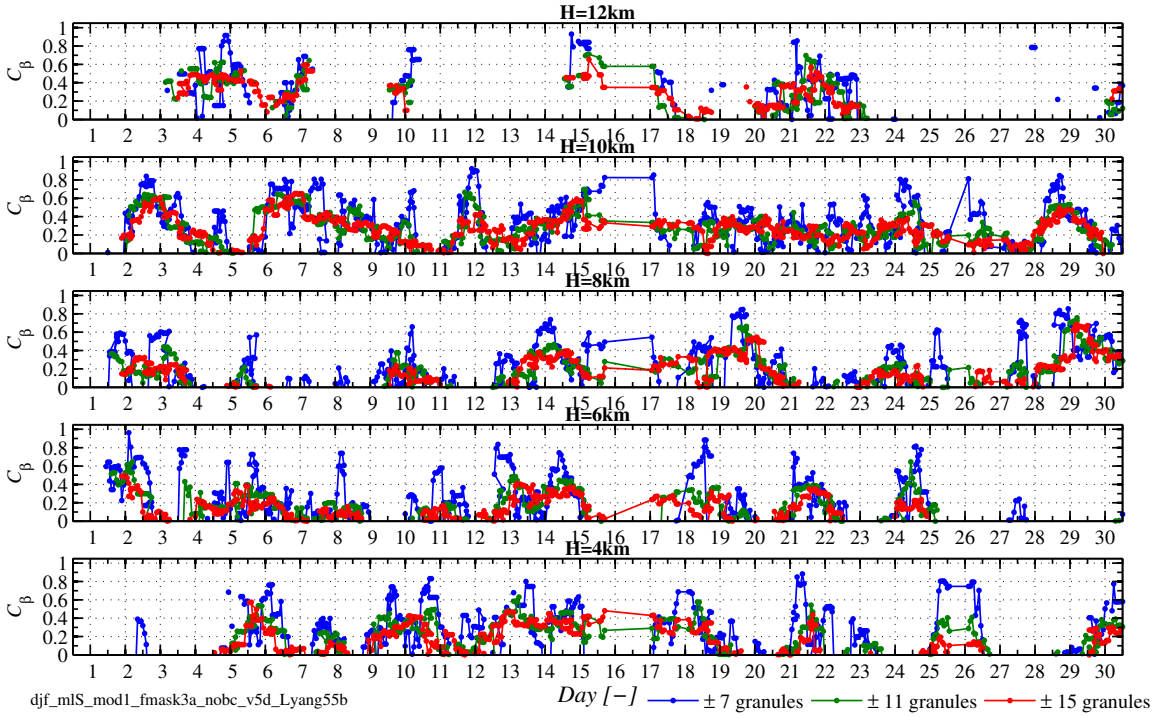

Figure 2.14: Time series of correlation between granule-mean CALIOP backscatter and IFS-ZmVar backscatter for the period from 1 to 30 January 2007, considering observations at mid-lat. South (30°S-60°S). Each line refers to the time length indicated in the legend. Different panels contains data at the altitude level (H) shown in the title.

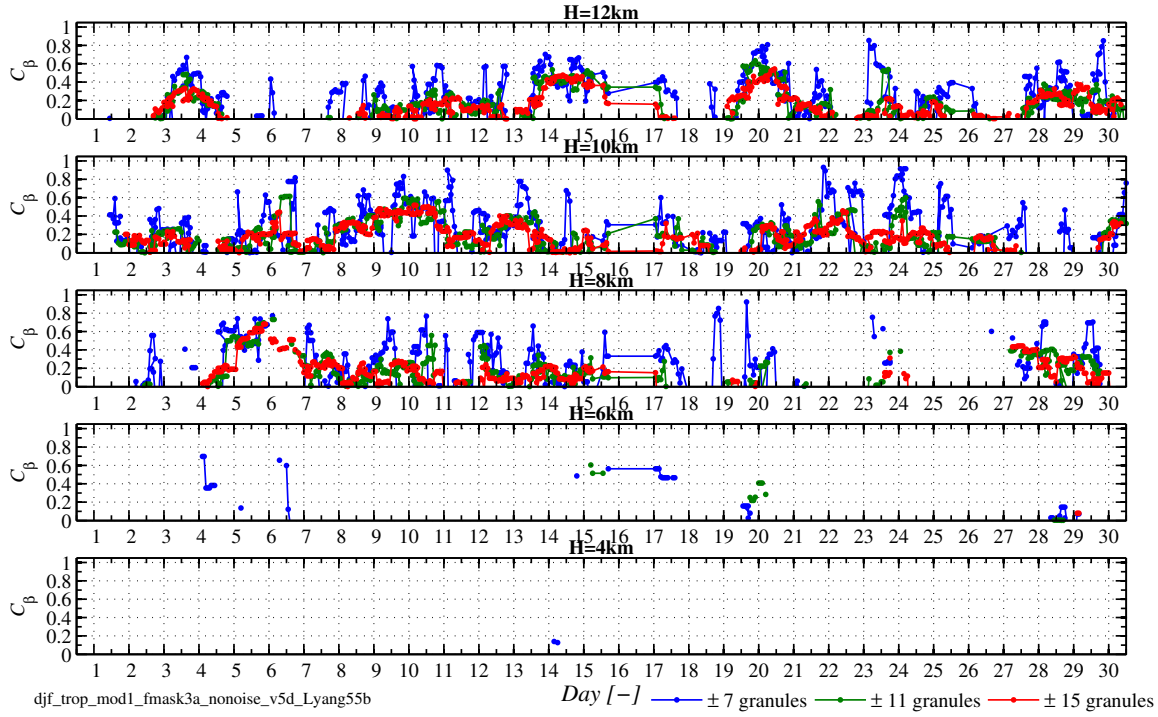

Figure 2.15: Same as Fig. 2.14, but considering observations in the tropics (30°S-30°N).

3 Monitoring of cloud-top height

Similarly to what was done in Di Michele et al. (2014a) for the CloudSat radar observations, the investigation of cloud-top height (CTH), derived from backscatter measurements, as monitoring variable, has also been done. First, stand-alone CTH derived from CALIOP measurements has been considered (Subsection 3.1), then CTH FG departures have also been taken into account (Subsection 3.2).

3.1 Time series of cloud-top height from CALIOP

CALIOP CTH h_{CA}^{top} can be defined as the altitude of the most high lidar bin with backscatter exceeding the molecular value β_{CA}^{mol}, i.e:

$$\beta_{CA}(h) < \beta_{CA}^{mol} \quad \forall h > h_{CA}^{top} \tag{3.1}$$

The value of β_{CA}^{mol} is determined from Collis and Russell (1976) using as input the FG temperature and pressure from the ECMWF forecasts. The CTH h_{CA}^{top} can be considered as a derived observation and therefore monitored using the same approach as for backscatter. Following the usual approach, the temporal evolution of h_{CA}^{top} statistics (mean, standard deviation, number of samples) has been evaluated over 30 days in July 2007, distinguishing the same two geographical regions as in Section 2. Time series of mean CTH, $\overline{h_{CA}^{top}}$ are shown in Fig. 3.1, where the top panel considers observations at Southern mid-latitudes and the bottom refers to tropical cases. In both regions it is evident that only the 24-hour averaging is able to reduce the rapid oscillations of the mean to values below one kilometre. One should note that the peak at day 12 in the 12-hour mean in the top panel (i.e. mid-latitudes) is due to only a portion of a single granule available for the averaging at that time.

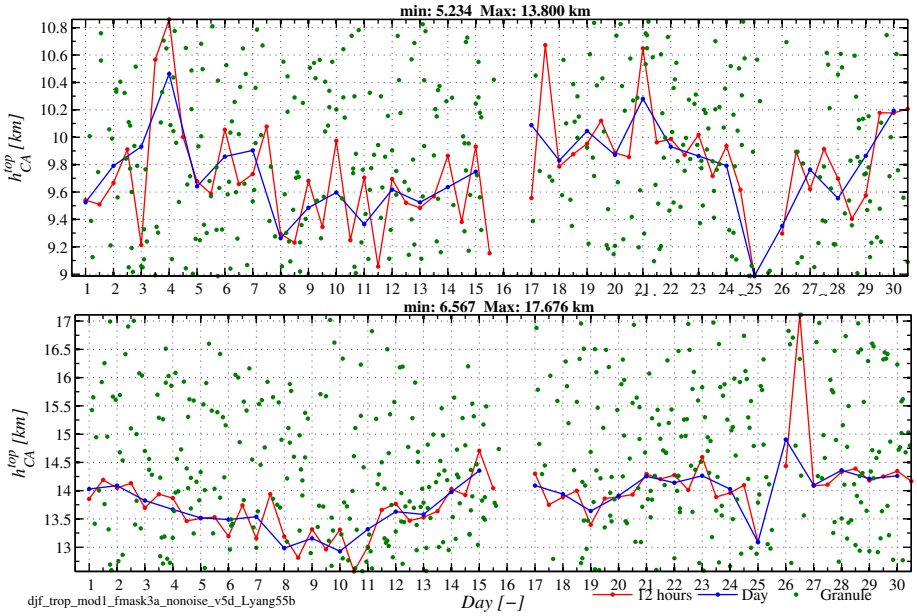

Figure 3.1: Time series of mean CALIOP-derived CTH for the period from 1 to 30 January 2007. Each line refers to the time window stepping indicated in the legend. Top panel is for observations at mid-latitudes South (30°S-60°S), and bottom panel uses observations in the tropics (30°S-30°N).

The corresponding temporal evolution of standard deviation $\sigma_{h_{CA}^{top}}$ is shown in Fig. 3.2. As for the mean, the standard deviation curves for granule and 12-hour mean evolve in time with strong oscillations. The comparison between the two regions indicate that the standard deviation in the tropics is overall larger (of about one kilometre) that at mid-latitudes. Similarly to backscatter, we can define an oscillation range $\Delta\overline{h_{CA}^{top}}$ of the mean CTH as the difference between maximum and minimum values in the monitoring period. Also, we can

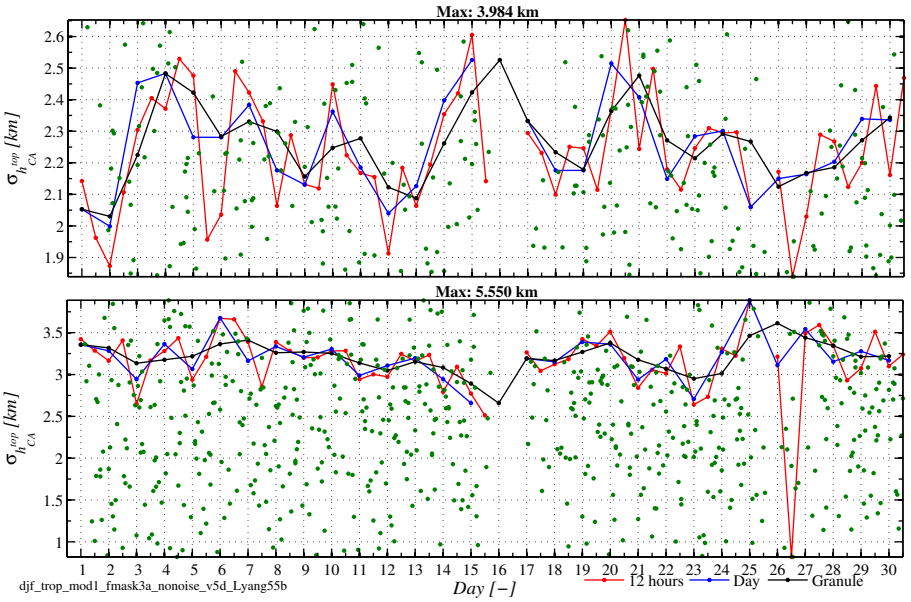

Figure 3.2: Same as 3.1, but for time series of standard deviation of CALIOP-derived CTH.

introduce the range of variation $\Delta\sigma_{h_{CA}^{top}}$ of the standard deviation. Their values corresponding to Fig. 3.1 and 3.2 are reported in Table 3.1. Figure 3.3 shows the number of h_{CA}^{top} samples $n_{h^{top}}$. Note that, in order not to take into account the data-drop periods, the 12-hour and day ranges have been evaluated discarding points having a number of samples lower than 1000 and 2000, respectively.

CALIOP	**Mid-Latitudes South**			**Tropics**		
-	*Granule*	*12 hours*	*Day*	*Granule*	*12 hours*	*Day*
$\Delta\overline{h^{top}}[km]$	12.337	2.729	1.800	15.754	3.323	2.477
$\Delta\sigma_{h^{top}}[km]$	5.537	0.909	0.716	8.204	1.224	0.877

Table 3.1: Oscillation range of mean and standard deviation CALIOP-derived CTH evaluated at different time windows.

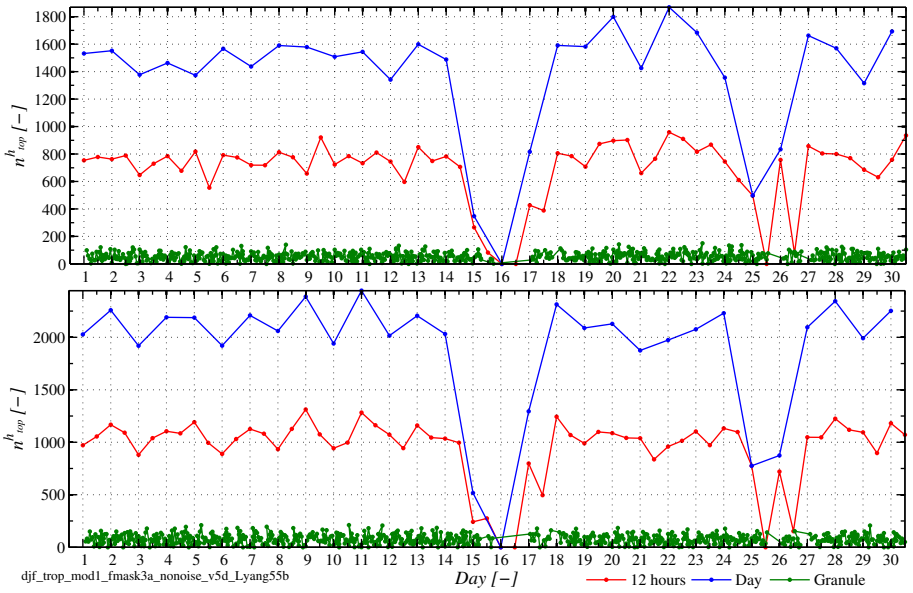

Figure 3.3: Same as 3.1, but for time series of number of samples of CALIOP-derived CTH.

3.2 Time series of cloud-top height departures

CTH departures δh^{top} have been generated evaluating the model counterpart to CALIOP CTH using the ZmVar lidar forward operator. Similarly to Eq. 3.1, CTHs from simulated backscatter h^{top}_{ZMV} have been computed as:

$$\beta_{ZMV}(h) < \beta^{mol}_{CA} \quad \forall h > h^{top}_{ZMV} \tag{3.2}$$

Figure 3.4 displays the CTH corresponding to backscatter shown in Fig 2.7. Generally, a good correlation seems to be between the CTH resulting from CALIPSO observations and the one derived from ZmVar backscatter based on the IFS forecast.

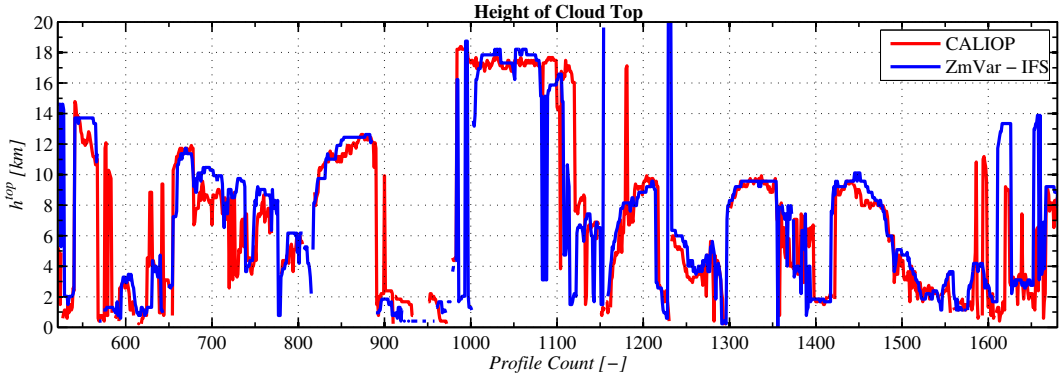

Figure 3.4: Height of cloud-top derived from CALIOP observations (red line) and from ZmVar cloud backscatter (blue line) corresponding to the data shown in Fig. 2.7.

Similarly as for the CloudSat derived CTH (Di Michele et al., 2014a), the assessment of the quality agreement between FG and observations is important when considering FG departures. The scatterplots between the CTH from CALIPSO and the one from the IFS forecast are shown for mid-latitudes and Tropics in Fig. 3.5 and Fig. 3.6, respectively. Those scatterplots are very similar to those ones obtained for CloudSat CTH (Fig. 3.4 - 3.5 in Di Michele et al., 2014a). Monitoring of the CTH departures corresponding to CALIOP has been performed in similar way as for the CloudSat ones using a screening to discard cases with the CTH departures larger than 5 km.

The results of monitoring CTH departures are given in Fig. 3.7 and Fig. 3.8, respectively for the mean $\overline{\delta h^{top}}$ and the standard deviation $\sigma_{\delta h^{top}}$. The time series of mean CTH FG departures show oscillations of few hundred meters, that are damped when averaging over one day and result in a bias constant in time. The standard deviation also presents a temporal evolution with rapid fluctuations, but the 12-hour averaging is already able to halve if to values below 1.5 km.

Table 3.2 summarizes the oscillation range of the mean CTH departure $\Delta\overline{\delta h^{top}}$ (evaluated as maximum minus minimum value) and the oscillation range of the standard deviation $\sigma_{\delta h^{top}}$, evaluated as the maximum-minus-minimum difference and maximum value on the 30 day period. Finally, Fig. 3.9 presents the correlation between the time evolution of granule-mean $\overline{h^{top}_{CA}}$ and $\overline{h^{top}_{ZMV}}$ evaluated using lengths of 5, 11, 15 granules. The remarkable agreement (consistent in time) between model and observations shown in these plots can be attributed to the ability of the model in reproducing the top of cloud. By comparison, the correlation curves in Fig. 2.14 and Fig. 2.15 are much worse because it is much more difficult to reproduce the full lidar backscatter profile in clouds. In fact, as already mentioned, small errors in the vertical structure of the modelled cloud can result in large discrepancies for the backscatter signal. In the case of CTH departures, the impact of errors coming from the lidar observation operator are lessen by using the simulated backscatter as in Eq. 3.2 contributing to very high correlation values for the CTH departures, especially in mid-latitudes.

CALIOP - IFS	Mid-Latitudes South			Tropics		
-	*Granule*	*12 hours*	*Day*	*Granule*	*12 hours*	*Day*
$\Delta\overline{\delta h^{top}}[km]$	2.292	0.520	0.260	5.481	1.201	0.391
$\sigma_{\delta h^{top}}[km]$	2.249	1.527	1.394	2.655	1.932	1.642

Table 3.2: Mean oscillation range and standard deviation of CALIOP-derived CTH FG departures evaluated at different time windows.

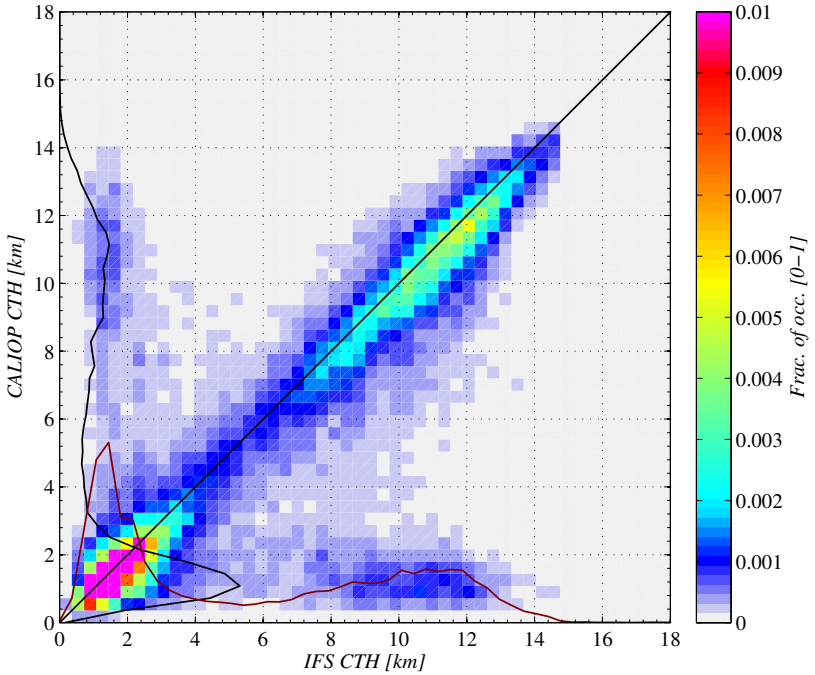

Figure 3.5: Scatter plot between cloud-top height derived from ZmVar cloud backscatter using the IFS model data as input (on abscissa) and the one derived from CALIOP (on ordinate) using observations over ocean matched with model data between 30°S and 60°S for the period of January 2007. Curves along axes show the relative occurrence of cloud-top height.

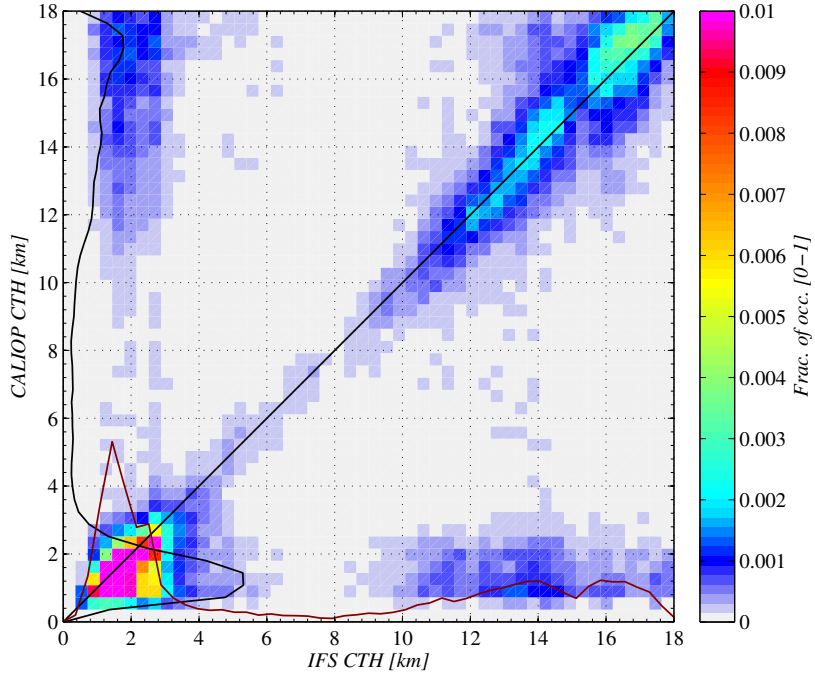

Figure 3.6: Same as 3.5, but considering observations in the tropics (30°S-30°N).

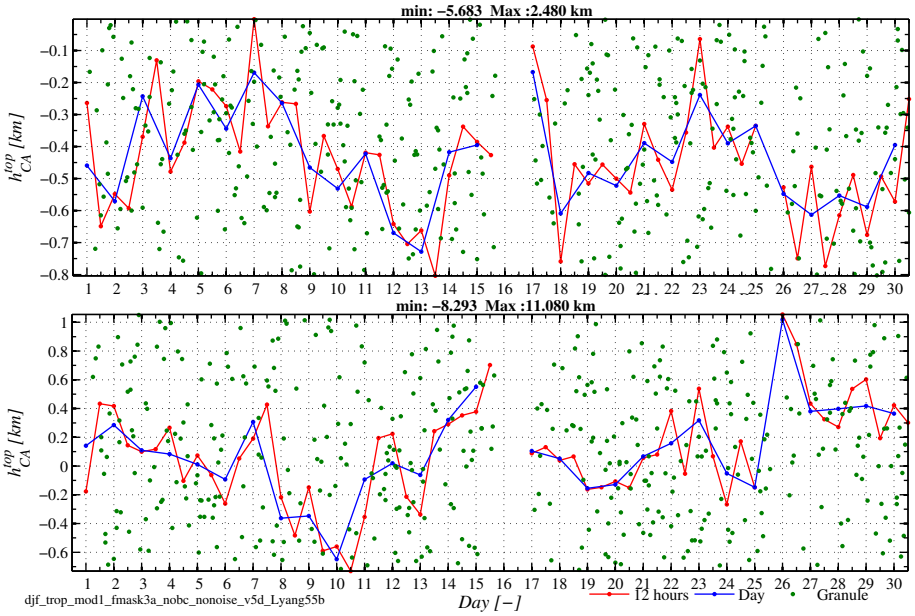

Figure 3.7: Same as 3.1, but for time series of CTH mean difference between CALIOP and IFS-ZmVar equivalents.

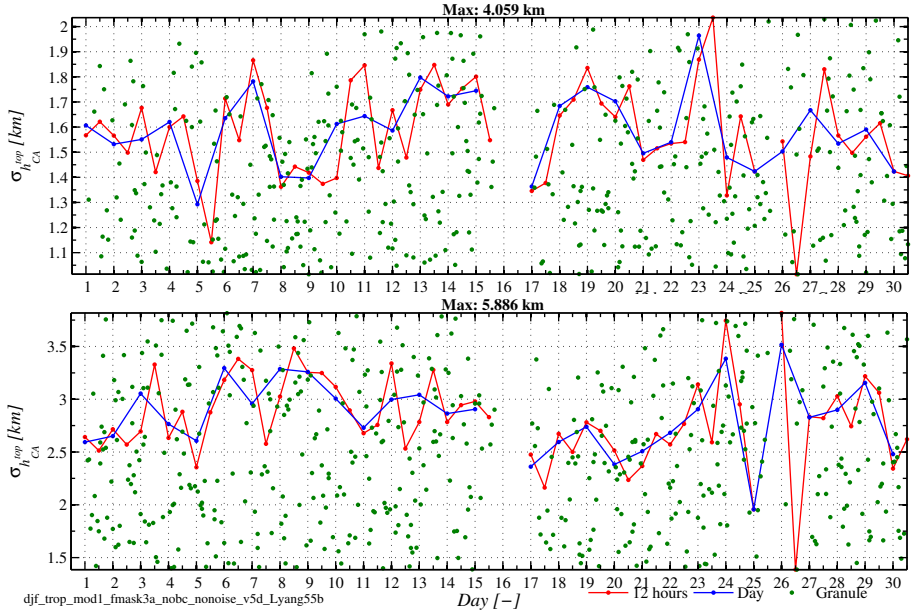

Figure 3.8: Same as 3.1, but for time series of standard deviation of CTH difference between CALIOP and IFS-ZmVar equivalents.

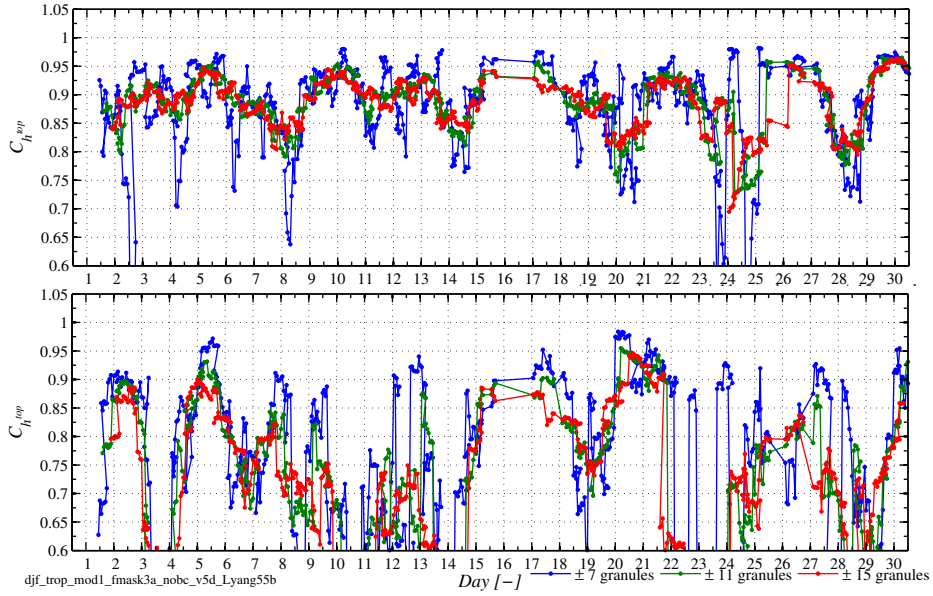

Figure 3.9: Time series of correlation between granule-mean CALIOP-derived and IFS-ZmVar derived CTH for the period from 1 to 30 January 2007. Each line refers to the time length used to evaluate the correlation as indicated in the legend. Top panel is for observations at mid-latitudes South (30°S-60°S), and bottom panel uses observations in the tropics (30°S-30°N).

4 Conclusions

Time series of CALIOP observations have been compared to their model equivalent. The performed studies have shown that, after applying a quality control screening, there is a certain degree of consistency between simulated and observed backscatter in clouds. The extra information brought by the forecast model can contribute to a reduction of the size of the minimum anomaly detectable through the continuous monitoring of the temporal evolution of statistical parameters for the differences between observations and their model equivalents.

A better agreement between observations and simulations has been shown when considering backscatter-derived CTH as monitoring variable. Monitoring of the CTH departures has revealed very high correlation between CALIOP-derived and ZmVar-derived CTH which can be related to the ability of the model to reproduce the top of cloud.

This study will be continued in WP-3100, considering more time periods and investigating the impact that possible glitches in the lidar signal have on the evolution of the monitored quantities.

Acknowledgements

The authors are grateful to the NASA Langley Research Center - Atmospheric Science Data Center for making the CALIPSO data available. Thanks are due to Anton Beljaars and Stephen English for helpful advice and review of the document.

List of Acronyms

4D-Var	Four-Dimensional Variational Assimilation
ATLID	ATmospheric LIDar
CALIOP	Cloud-Aerosol Lidar with Orthogonal Polarization
CALIPSO	Cloud-Aerosol Lidar and Infrared Pathfinder Satellite Observation
CloudSat	NASA's cloud radar mission
CTH	Cloud Top Height
EarthCARE	Earth, Clouds, Aerosols and Radiation Explorer
ECMWF	European Centre for Medium Range Weather Forecasts
ESA	European Space Agency
FG	First Guess
GCM	Global Circulation Model
IFS	Integrated Forecasting System of ECMWF
NASA	National Aeronautics and Space Administration
NWP	Numerical Weather Prediction
QuARL	Quantitative Assessment of the operational value of space-borne Radar and Lidar measurements of cloud and aerosol profiles
SMOS	Soil Moisture and Ocean Salinity mission
STSE	Support-to-Science-Element
USN	Universal Space Network
ZmVar	Z (reflectivity) Model for Variational assimilation of ECMWF

References

Collis, R. and P. Russell, 1976: Lidar measurement of particles and gases by elastic backscattering and differential absorption, *Laser monitoring of the atmosphere*, pp. 71–151.

Di Michele, S., E. Martins, and M. Janisková, 2014a: Monitoring of radar data, WP-2100 report for the project Support-to-Science-Element STSE Study - EarthCARE Assimilation, 4000102816/11/NL/CT, ECMWF, 22 pp.

Di Michele, S., E. Martins, and M. Janisková, 2014b: Observation operator and observation processing for cloud lidar, WP-1200 report for the project Support-to-Science-Element STSE Study - EarthCARE Assimilation, 4000102816/11/NL/CT, ECMWF, 40 pp.

Hollingsworth, A., D. Shaw, P. Lönnberg, L. Illari, K. Arpe, and A. Simmons, 1986: Monitoring of observation and analysis quality by a data assimilation system, *Mon. Weather Rev.*, **114**, 861–879.

Janisková, M., O. Stiller, S. Di Michele, R. Forbes, J.-J. Morcrette, M. Ahlgrimm, P. Bauer, and L. Jones, 2010: QuARL - Quantitative Assessment of the Operational Value of Space-Borne Radar and Lidar Measurements of Cloud and Aerosol Profiles, ESA Contract Report on Project 21613/08/NL/CB, 329 pp.

Liu, Z., M. Vaughan, D. Winker, C. Kittaka, B. Getzewich, R. Kuehn, A. Omar, K. Powell, C. Trepte, and C. Hostetler, 2009: The CALIPSO lidar cloud and aerosol discrimination: Version 2 algorithm and initial assessment of performance, *J. Atmos. and Ocean. Tech.*, **26**(7), 1198–1213.

Muñoz Sabater, J., M. Dahoui, P. de Rosnay, and L. Isaksen, 2012: ESA/ESRIN Contract 4000101703/10/NL/FF/fk Technical Note Phase II, WP1100: SMOS Monitoring Report. Number 2: Nov 2010 - Nov 2011, Technical Report, ECMWF.

Stephens, G., D. Vane, R. Boain, G. Mace, K. Sassen, Z. Wang, A. Illingwort, E. O'Connor, W. Rossow, and S. Durden, 2002: The CloudSat mission and the A-train, *Bull. Am. Meteorol. Soc.*, **83**(12), 1771–1790.

Vaughan, M., K. Powell, R. Kuehn, S. Young, D. Winker, C. Hostetler, W. Hunt, Z. Liu, M. McGill, and B. Getzewich, 2009: Fully Automated Detection of Cloud and Aerosol Layers in the CALIPSO Lidar Measurements, *J. Atmos. and Ocean. Tech.*, **26**(10), 2034–2050.

Winker, D., M. Vaughan, A. Omar, Y. Hu, K. Powell, Z. Liu, W. Hunt, and S. Young, 2009: Overview of the CALIPSO mission and CALIOP data processing algorithms, *J. Atmos. and Ocean. Tech.*, **26**(7), 2310–2323.